PCCP

PAPER

View Article Online
View Journal | View Issue

Cite this: *Phys. Chem. Chem. Phys.*, 2016, **18**, 2850

Diverse interface effects on ferroelectricity and magnetoelectric coupling in asymmetric multiferroic tunnel junctions: the role of the interfacial bonding structure

X. T. Liu,[ab] W. J. Chen,[abc] G. L. Jiang,[ab] B. Wang[ac] and Yue Zheng*[ab]

Received 1st September 2015,
Accepted 14th December 2015

DOI: 10.1039/c5cp05207f

www.rsc.org/pccp

Interface and size effects on electric/magnetic orders and magnetoelectric coupling are vital in the modern application of quantum-size functional devices based on multiferroic tunnel junctions. In order to give a comprehensive study of the interface and size effects, the properties of a typical asymmetric multiferroic tunnel junction, *i.e.*, Fe/$BaTiO_3$/Co, have been calculated using the first-principles simulations. Most importantly, all of the eight possible structures with four combinations of electrode/ferroelectric interfaces (*i.e.*, Fe/BaO, Fe/TiO_2, Co/BaO and Co/TiO_2) and a series of barrier thicknesses have been taken into account. In this work, the equilibrium configurations, polarization, charge density, spin density and magnetic moments, *etc.*, have been completely simulated and comprehensively analyzed. It is found that the ferroelectric stability is determined as a competition outcome of the strength of short-range chemical bondings and long-range depolarization/built-in fields. M/BaO (M = magnetic metal) terminations show an extraordinary enhancement of local polarization near the interface and increase the critical thickness of ferroelectricity. The bistability of polarization is well kept at the M/TiO_2 interface. At the same time, the induced magnetic moment on atoms at the interfaces is rather localized and dominated by the local interfacial configuration. Reversing electric polarization can switch the induced magnetic moments, wherein atoms in M–O–Ti and M–Ti–O chains show preference for being magnetized. In addition, the difference between the sum of the interfacial magnetic moments is also enlarged with the increase of the barrier thickness. Our study provides a comprehensive and detailed reference to the manipulation and utilization of the interface, size and magnetoelectric effects in asymmetric multiferroic tunnel junctions.

1. Introduction

Multiferroic tunnel junctions (MFTJs) have become the objects of much scientific importance for their promising applications in spintronic devices for non-volatile memory and sensor applications, especially magnetic and ferroelectric ones.[1–5] Constructed by two magnetic electrodes sandwiched with a ferroelectric layer, MFTJs exhibit novel effects such as the tunneling magnetoresistance (TMR) effect,[6–8] the giant electroresistance (GER) effect[9–11] and the four resistant state,[5,12] which means that the conductance of the junction can be tuned by exerting magnetic or electric field. In such a laminar nanostructure, the properties of the junction show great dependence on the size of the ferroelectric barrier and the specific interfacial structures. In most ferroelectric ultra-thin films, it has been found that the spontaneous polarization is suppressed due to the effect of the depolarizing field and ferroelectricity disappears when the film is below a critical thickness, leading to a fatal failure of ferroelectric devices. That makes the stability of ferroelectricity an important issue to be discussed. In latest works, the critical thickness of ferroelectricity has been lowered down to one or a few nanometers in experiment works[13,14] and theoretical works,[15–18] and the critical thickness of the spontaneous polarization even vanishes in some cases predicted by the first principles calculations.[11,19,20] In the determination of ferroelectric stability of nanoscale tunnel junctions, the interfacial features play vital roles. It has been commonly accepted that this is due to the depolarization field generated from uncompensated or partially compensated bound charges at the interface.[10] Thus the specific details of atom positions, charge transfer and chemical bondings at the interface, along with thin film thickness, will significantly affect the behavior of ferroelectricity. Early works on thin film bilayers or symmetric tunnel junctions

[a] *State Key Laboratory of Optoelectronic Materials and Technologies, School of Physics and Engineering, Sun Yat-sen University, 510275, Guangzhou, China. E-mail: zhengy35@mail.sysu.edu.cn; Tel: +86 8411-3231*
[b] *Micro&Nano Physics and Mechanics Research Laboratory, School of Physics and Engineering, Sun Yat-sen University, 510275, Guangzhou, China*
[c] *Sino-French Institute of Nuclear Engineering and Technology, Sun Yat-sen University, Zhuhai, 519082, China. E-mail: wangbiao@mail.sysu.edu.cn; Tel: +86 8411-5692*

figure out that the interfaces having a stronger screening effect lead to more stable ferroelectric distortion.[17,20] Latest works on asymmetric tunnel junctions show that though the bistability of the ferroelectric thin film exists only when the thin is thick enough, the critical thickness of the spontaneous polarization vanishes. Some particular tunnel junctions have zero critical thickness of ferroelectricity. There are two contributing factors in the enhancement of ferroelectric stability. One is the built-in field generated by the contact potential difference of two electrode/thin film interfaces, which are the long-range effect.[11,19–26] The other is the local bonding and mechanical environment that is well kept at the interfaces but may lead to collective response in the vicinity, which is the short-range effect.[20,27] These two factors both involve the specific interface structures and the thickness of the ferroelectric film, making it necessary to investigate the influence of different magnetic/ferroelectric interfaces and the size effect.

Apart from the above, the coupling of ferroelectricity and magnetization in MFTJs enables the magnetic (electric) control of ferroelectricity (magnetism), which is defined as the magnetoelectric (ME) effect.[2,28,29] For instance, Pantel *et al.*[30] found that reversing the polarization can switch TMR from −7% to 5% instantaneously. As the ferroelectric stability significantly affects the interfacial bonding structure *via* the formation of an electric dipole, and the ME effect in multiferroic layered composites is highly sensitive to the specific structure of the magnetic/ferroelectric interface, consequently, the ME effect can be adjusted by manipulating the electric polarization. There are three mechanisms in the decision of the interfacial ME effect: first, the interfacial atoms' positions altered by the ferroelectric polarization change the chemical bonding and hybridization at the ferroelectric/magnetic interface, resulting in a difference in the spin splitting of electron states as well as interfacial magnetization.[15,31–33] Second, in doping systems, the accumulation of spin-polarized electrons or holes redistributes due to ferroelectric polarization, and consequently affects the magnetization at the interface.[34,35] Third, the magnetization and ferroelectric polarization couple indirectly *via* the mediation of strain, that is, for example, strain as a response to the ferroelectric polarization by the inverse piezoelectric effect will lead the magnetization to change by magnetostriction.[36] In most of the magnetic/ferroelectric interface, the last two mechanisms have little influence, while the first mechanism, also named as the interface chemistry mechanism, plays the dominant role.

Though a great quantity of research works has been done to investigate the origin and mechanism of the magnetoelectric properties of MFTJs, the behavior of MFTJs concerned with a series of comparable interface structures has rarely been investigated. Our previous work only investigated the ferroelectric stability and the magnetoelectric effect in the tunnel junctions terminated by symmetric layers, and explained the influence of the built-in field generated by the difference of contact potentials at the interfaces.[21] As both TiO_2- and BaO-terminated surfaces can be found in $BaTiO_3$ thin films,[37] eight possible structures with four combinations of electrode/ferroelectric interfaces (*i.e.*, Fe/BaO, Fe/TiO_2, Co/BaO and Co/TiO_2) and a series of the barrier thicknesses for asymmetric Fe/$BaTiO_3$/Co heterostructures are taken into account in this work. We investigate the interfacial control of magnetoelectric properties of MFTJs by performing first-principles simulations, whose results can be extended to general M1/ABO_3/M2 MFTJs (M for the magnetic electrode and ABO_3 for perovskite ferroelectrics). We demonstrate how the ferroelectric stability is affected by the thickness of the ferroelectric barrier and the dissimilar magnetic/ferroelectric interfaces, and how the magnetic properties at the interfaces are coupled with the ferroelectric polarization. Our results of simulations also provide a comprehensive picture of the ferroelectric control of magnetization in MFTJs.

2. Simulation methods

We perform the calculations within the spin-polarized density-functional theory (DFT) as implemented in the Vienna *ab initio* Simulation Package (VASP).[38] The projector augmented wave (PAW) method and a plane-wave basis set are employed.[39] The exchange–correlation potential is treated in the local density approximation (LDA). The Perdew–Zunger (PZ) interpolation formula is used for the correlation part of the exchange correlation.[40] The plane wave functions are expanded with an energy cutoff of 500 eV. For structural relaxation, we use a converged 6 × 6 × 1 Monkhorst–Pack grid for *k*-point sampling with a 0.2 eV Gaussian broadening. All the atoms are relaxed using until the Hellmann–Feynman force on each atom is less than 20 meV $Å^{-1}$. Following that, we adopt a denser *k*-point mesh of 18 × 18 × 2 in static calculations to obtain the static properties including charge density, spin density and density of states (DOS).

The MFTJs are simulated to be epitaxially grown on the $SrTiO_3$ (001) substrate by constraining the in-plane lattice constant of the supercell to the theoretical bulk lattice constant of $SrTiO_3$ (3.866 Å). Relaxation of bulk tetragonal face centered Fe, Co and perovskite $BaTiO_3$ (without ferroelectric distortion) lattices is performed under this in-plane lattice constraint. The relaxed tetragonal unit cells of the bulk Fe, Co and $BaTiO_3$ are then used as building blocks for the supercells. The Fe, $BaTiO_3$ and Co layers are stacked along the [001] direction (*z* direction) of the bulk counterparts. Therefore, the supercells are considered in the perpendicular direction to the transport direction. The short-circuit boundary condition is naturally introduced by constructing a superlattice under periodic boundary conditions. To simulate a practical situation where the magnetizations of the two electrodes of a MFTJ are either parallel or anti-parallel, in this work we exclusively consider a collinear spin-polarized system. A non-collinear spin-polarized system with the magnetizations of the two electrodes canted with an angle should be interesting and will be explored in a future work. The relative orientation of the magnetization of electrodes is realized by initializing the signs of the magnetic moments of electrode atoms. The values of the initial magnetic moments are tested to ensure converged equilibrium magnetic moments that are obtained from the self-consistent spin densities.

To give a comprehensive insight into the influence of electrode/ferroelectric interfaces, four possible types of MFTJs

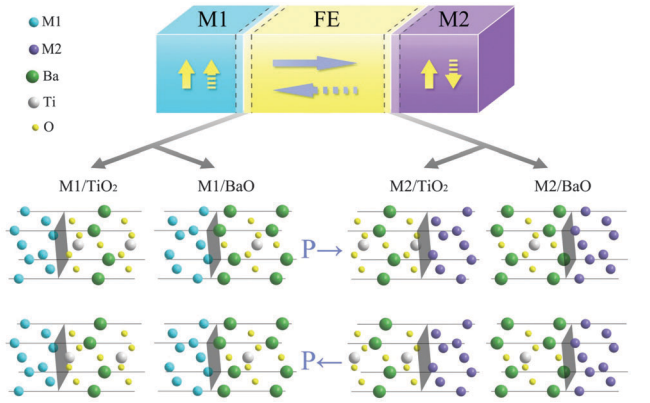

Fig. 1 Schematic structures and interfacial atomic structures of M1/FE/M2 MFTJs. Periodic boundary condition is employed in all three dimensions. Two orientations of electric polarization are considered, as indicated by the solid and dash blue arrows, respectively. Parallel and antiparallel magnetization of electrodes are considered, as indicated by the solid and dash yellow arrows, respectively.

with different combination of termination of ferroelectric layers are studies. According to our calculation results as well as previous reports of interfacial work of separation, in perovskite ferroelectric thin films sandwiched by simple metal electrodes, for both AO and BO_2 terminations, the structure that O lies on the top site of the metal atom is most energetically preferable.[41,42] The schematic structures of these tunnel junctions and the interface atomic configurations are depicted in Fig. 1. The MFTJs are constructed as Fe/TiO_2–(BaO–TiO_2)$_m$/Co, Fe/(BaO–TiO_2)$_m$/Co, Fe/BaO–(BaO–TiO_2)$_m$/Co and Fe/(BaO–TiO_2)$_m$/Co, where m ranges from 2 to 15 and the metal electrodes are fixed to a thickness of 4 unit cells. For convenience, in the following, we denote the above four structures by TT, TB, BB and BT, in turn.

To obtain the equilibrium ferroelectric geometry of the MFTJs, we first impose an initial displacement of Ti atoms along the [001] direction with respect to the O atoms in the same x–y plane, and then fully relax all of the atoms in the supercell. To be clear, the z direction pointing from the Fe/$BaTiO_3$ interface to the Co/$BaTiO_3$ interface, *i.e.* from left to right, is defined as positive. $P_0\rightarrow$ and $P_0\leftarrow$ denote the positive and negative initial ferroelectric distortion, respectively. Similarly, M↑↑ and M↑↓ denote parallel and antiparallel magnetization of the two electrodes, respectively. The local polarization P of MFTJs is evaluated according to the formula $P = e\sum Z_i^* u_i/V$, where e is the electronic charge, Z_i^* is the Born effective charge of ion i, u_i is the displacement of the ion i in the ferroelectric state with respect to the paraelectric state and V is the volume of the unit cell. Using the Berry phase method, the calculated Born effective charges are 2.71 and 6.62 for Ba and Ti, respectively, and −5.02 and −2.08 for O in the BaO and TiO_2 planes, respectively.

3. Results and discussion

3.1 Ferroelectric stability and its size dependence

We first study the ferroelectric stability and its size dependence of the asymmetric MFTJs. Fig. 2–5 present the layer-resolved relative Ba–O and Ti–O displacements at the [001] $BaTiO_3$ monolayers and the calculated average polarization for four types of the tunnel junctions. It has to be mentioned that the equilibrium structures for two magnetization configurations are similar with a negligible difference, so we present the results of parallel magnetization.[21] For TT tunnel junctions as shown in Fig. 2, the smaller Ti–O displacements near the interfaces not only validate the suppressing effect on ferroelectricity by the depolarization field, but also imply that the interaction between TiO_2 layers and the electrode interfacial atoms is relatively weak. Besides, when $m < 5$, the relaxed Ti–O relative displacements are all negative despite the signs of initial Ti–O displacements, *i.e.*, the P→ state is unstable and will spontaneously reverse to the P← state as shown in Fig. 2c and d. Given the definition that the critical thickness of polarization bistability (CTPB) is a thickness below which the polarization is stable in only one direction, the CTPB of the TT structure is $m = 5$. This result is consistent with previous reports about asymmetric FTJs.[20] The existence of CTPB is originated from the built-in field generated by the difference of the contact potentials at the two interfaces.[21] As for the TB structure in Fig. 3, Co/BaO termination shows a strong enhancement of interfacial polar distortion with a magnitude of ∼0.3 Å, pointing

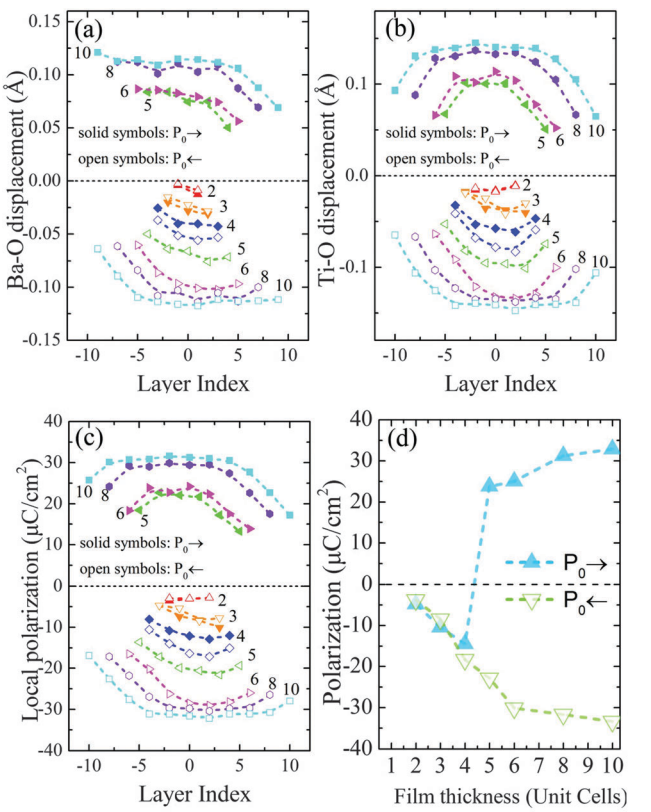

Fig. 2 Ferroelectric stability in the Fe/TiO_2–(BaO–TiO_2)$_m$/Co MFTJs for different thicknesses of $BaTiO_3$ films. (a–d) Corresponds the relative Ba–O displacement at [001] BaO monolayers, the relative Ti–O displacement at [001] TiO_2 monolayers, the local polarization, and the equilibrium average polarization as a function of film thickness. The layer index is set to be zero at the middle of the barrier.

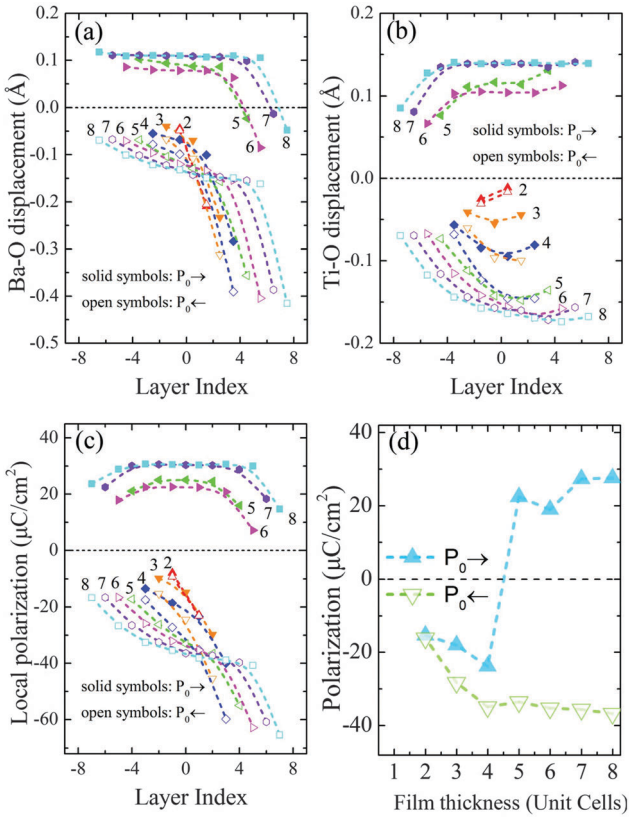

Fig. 3 Ferroelectric stability in the Fe/$(TiO_2$–$BaO)_m$/Co MFTJs for different thicknesses of $BaTiO_3$ films. (a–d) Corresponds the relative Ba–O displacement at [001] BaO monolayers, the relative Ti–O displacement at [001] TiO_2 monolayers, the local polarization, and the equilibrium average polarization as a function of film thickness. The layer index is set to be zero at the middle of the barrier.

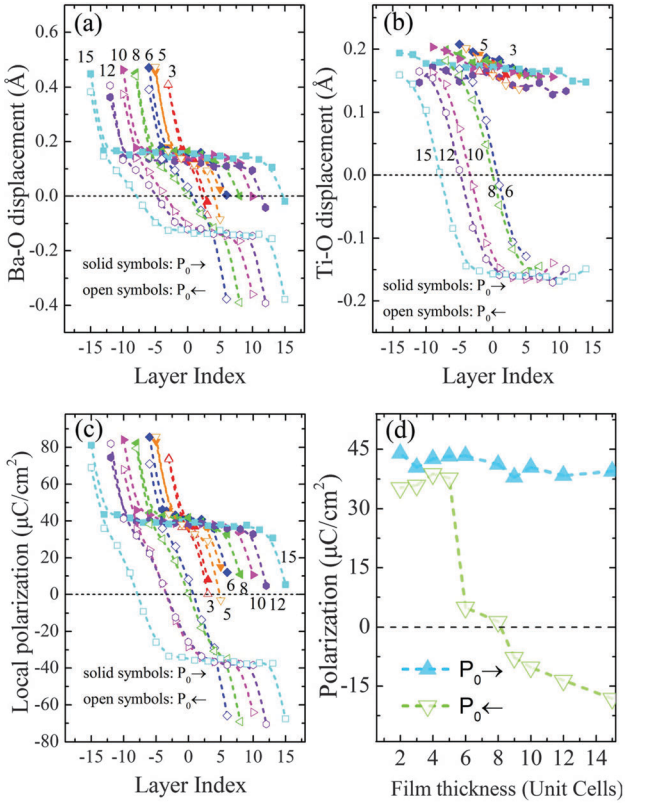

Fig. 4 Ferroelectric stability in the Fe/BaO–$(TiO_2$–$BaO)_m$/Co MFTJs for different thicknesses of $BaTiO_3$ films. (a–d) Corresponds the relative Ba–O displacement at [001] BaO monolayers, the relative Ti–O displacement at [001] TiO_2 monolayers, the local polarization, and the equilibrium average polarization as a function of film thickness. The layer index is set to be zero at the middle of the barrier.

from the electrode to the ferroelectric film. It demonstrates that the change of the interfacial structure does weaken the bistability of the polarization at the interface. The CTPB of the TB structure is obtained as m = 5, as the same as TT structure, implying that the impact on ferroelectric bistability of Co/BaO is commensurate with that of Co/TiO_2. As for the BB structure in Fig. 4, from the results about the Fe/BaO interface, the tendency of Ba–O distortion to point away from the electrode is further confirmed. Not only the CTPB increases to m = 6, but also the dipole is "pinned" positively at the Fe/BaO interface in spite of the direction of initial ferroelectric distortion. Along with this, the neighbor Ba–O and Ti–O displacements point away from the electrode even when the overall polarization is opposite, that means the Fe/BaO interface can cause a non-switchable collective ferroelectric distortion and form a mono-stable electric domain about 3 unit cells thick. As for the BT structure in Fig. 5, the non-switchable polarization at the Fe/BaO interface and the bistable polarization at the Co/TiO_2 interface together lead the CTPB to increase to m = 12.

Comparing Fig. 3–5 with Fig. 2, a Ba–O relative displacement with a larger magnitude of ~0.4 Å is observed at every M/BaO interface, presenting the strong tendency to point away from the electrode. More interestingly, the local electric polarization can reach as large as 60 μC cm^{-2}, which is 50% higher than the saturation polarization at the center of the ferroelectric thin film. The strong interfacial enhancement in the AO-terminated perovskite ferroelectrics can be interpreted in terms of local chemical bonding. A shorter distance between M and O enables lower energy due to the attractive M–O bond and repulsive M–A/M–B bonds, the difference in the force constants makes the difference in the ferroelectric stability. As a result, the A–O dipole pointing away from the electrode is far more stable. The stability of the enhancement of interfacial ferroelectricity depends on the strength of the M–O bond, which was also explained by Stengel *et al.*[27] In order to give a quantitative analysis, we also calculated the longitudinal force constants of M–O interfacial bondings by the definition. At the BaO interface, k_{Fe-O} and k_{Co-O} are obtained as 0.028 a.u. and 0.026 a.u., respectively, which indicates instability of M–O bonding at the BaO interface and a strong tendency for the Ba–O fixed dipole to exist.

3.2 Charge and spin redistributions at the interfaces

To give an intuitionistic picture of the charge and spin redistributions at the interfaces, we present the differential charge density and the differential spin density. Such densities denote the difference between the self-consistent charge (spin) density and the non-self-consistent one, *i.e.*, a superposition of the

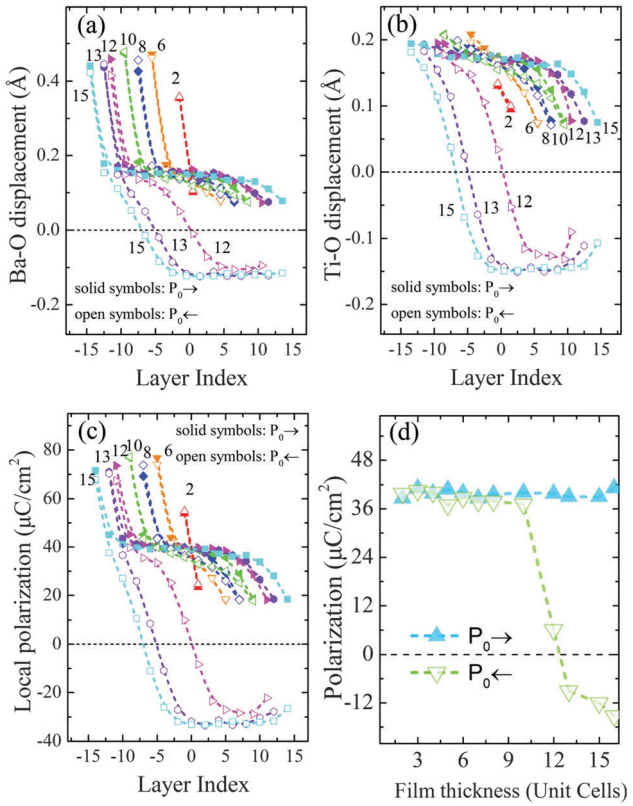

Fig. 5 Ferroelectric stability in the Fe/(BaO-TiO_2)$_m$/Co MFTJs for different thicknesses of $BaTiO_3$ films. (a–d) Corresponds the relative Ba–O displacement at [001] BaO monolayers, the relative Ti–O displacement at [001] TiO_2 monolayers, the local polarization, and the equilibrium average polarization as a function of film thickness. The layer index is set to be zero at the middle of the barrier.

charge (spin) density of stand-alone atoms. We take differential charge density and the differential spin density on the (010) plane for analysis as depicted in Fig. 6a and b, respectively. One can see that the local features of the electronic environment are well kept at the similar interfaces. For example, the differential charge densities at the Fe/TiO_2 interface in the TT structure and the TB structure show no obvious difference. Therefore, the results in Fig. 6a and b are presented according to the termination combination.

The differential charge density shown in Fig. 6a explains the origin of the robust distortion at the M/BaO interfaces. At these interfaces, both Ba atoms and M atoms are inclined to losing electrons, so that the direct contact makes each of them experience a significant repulsive force from each other, while O atoms and M atoms attract each other. As a consequence, the local polarization at the M/BaO interface always persists, in spite of the direction of overall polarization in the ferroelectric barrier, or even induces a collective ferroelectric distortion. At the M/TiO_2 interfaces, the simulation also revealed that the differential charge around the interfacial atom is opposite to that around the neighbor interfacial atom, making the force on atoms relatively even. These results are consistent with conclusions in Stengel's work[27] and Chen's[20] work, which also predicted the enhancement of ferroelectricity at the AO-terminated perovskite ferroelectrics.

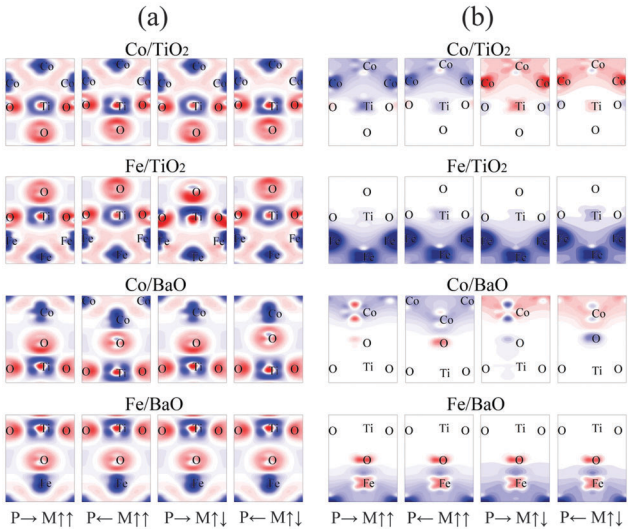

Fig. 6 Differential charge density (a) and differential spin density (b) in the x–z plane of the Fe/$BaTiO_3$/Co supercell in four magnetoelectric states as indicated at the bottom. Red refers to the positive value and blue refers to the negative value.

From the differential spin density shown in Fig. 6b, one can see that the spin redistributions are quite different for the four types of interfaces, even for interfaces (*e.g.*, the M/BaO interfaces) having the same termination of the $BaTiO_3$ barrier. For each type of interface, there is a small amount of spin transferring from the magnetic electrodes into the nonmagnetic $BaTiO_3$ barrier. Particularly, the spin transferring is more significant in the Fe/$BaTiO_3$ interfaces than the Co/$BaTiO_3$ interfaces. For the M/BaO interfaces, both the interfacial M atoms and O atoms have an increase in spin density. Meanwhile, for the M/TiO_2 interfaces, the spin density of M atoms decreases, and spin is induced at Ti atoms with its sign opposite to that of M atoms. It can also be seen that the spin splitting of ferroelectrics is highly localized, which happens almost only at the interface monolayer.

3.3 Magnetic moments of interfacial atoms

To quantitatively analyze the magnetic properties of interfaces, the magnetic moments of the atoms at interfaces are further calculated. Consistent with the result in Fig. 6, we found that the magnetic moments of M and O all increase at the M/BaO interfaces, making the magnetic moments of the same sign. At the M/TiO_2 interfaces, the magnetic moments of M decrease while the magnetic moments of Ti are of the opposite sign of magnetization of M. The absolute values of magnetic moments of some interfacial atoms are displayed in Fig. 7. One can see that barrier atoms (*i.e.*, Ti, Ba and O) at the interface possess net magnetic moments despite their zero initial spins. Magnetic moments of Fe and Co all differ from their tetragonal bulk values (1.9 μ_B and 1.6 μ_B, respectively), consistent with the differential spin density results in Fig. 6b.

It should be noted that magnetic moments of Ba in the BaO layer and O in the TiO_2 layer (denoted as O_{Ti} for convenience) are negligible with a maximum value of $\sim$0.05 μ_B even at the

interfacial layer, while Ti possesses a magnetic moment of about 0.02 μ_B even at the sub-interfacial layer. The distinction between the ability of different atoms to be magnetically polarized can be explained from the distribution of density of states. Fig. 8 shows the orbital-resolved density of states for atoms at the Co/TiO_2 interface and the Co/BaO interface, which can be easily expanded to the Fe case. The susceptible nature of Ti to magnetization is originated from the hybridization of the 3d electric orbitals of Ti atoms and simple metal atoms,[15] as can be seen in Fig. 8 as a protrusion occurs at −1.2 eV. For Ba, the outermost 5d electronic orbitals are full, making it too stable to be spin polarized. The magnetic moment of O atoms is sensitive to their position. At the M/BaO interface, O in the BaO layer (denoted as O_{Ba} for convenience) contacts directly with M and in a straight line with Ti and M. The O 2p orbital shifts to higher energy with a peak at −1.2 eV and serves as a medium for d electrons to transfer between M and Ti. At the M/TiO_2 interface, the full d orbital of Ba prevents double-exchange from happening, making O_{Ti} relatively weakly spin-polarized.

3.4 Magnetoelectric effect

From the results above, it is clear that the magnetic moments of atoms near the interface can be switched by the reversal of the polarization. To quantify the interfacial dependence of the magnetoelectric effect, the magnetoelectric coefficients for all types of terminations have been studied. The magnetoelectric coefficient is defined as $\alpha_s = \partial H/\partial E = \mu_0 \Delta M/E$, where μ_0 is the vacuum permeability, ΔM is the change in magnetization and E is the applied electric field. Duan *et al.*[15,28] have suggested a method to treat electric field E as the coercive electric field E_c and ΔM as the difference of total magnetic moments per unit cell between the top and bottom interfaces. However, as the above reports are based on symmetric junctions, some modification is needed to extend this method to our asymmetric systems. First, we calculated the difference between magnetization (in units of G) at the interface for the P→ state and for the P← state rather than for the two interfaces in the same structure. Table 1 shows the results of typical polarization-bistable structures. The results of these asymmetric MFTJs are of the same order as $\mu_0\Delta M$ = 120 G in the Fe/$BaTiO_3$ bilayer in Duan's report,[15] and are without doubt larger $\mu_0\Delta M$ = 0 in symmetric junctions. The calculated results show a remarkable distinction between M↑↑ and M↑↓ states and for different termination combinations, whose mechanism will be discussed later.

Although the coercive fields E_c of $BaTiO_3$ films are taken as 1–100 kV cm^{-1} in some theoretical reports, it is in fact

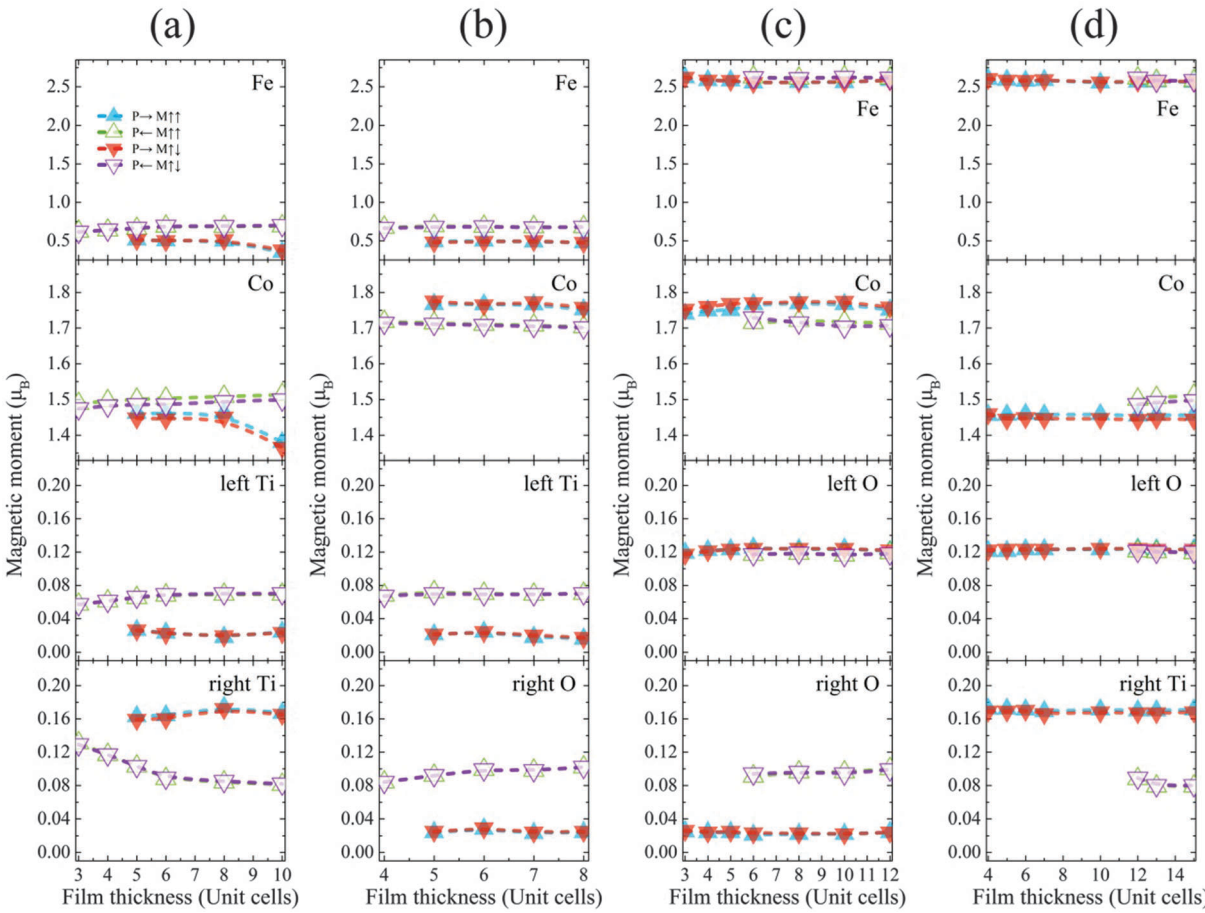

Fig. 7 Absolute values of magnetic moments of atoms at the very interfaces for MFTJs with different film thicknesses. (a–d) Corresponds to Fe/TiO_2–$(BaO–TiO_2)_m$/Co, Fe/$(TiO_2–BaO)_m$/Co, Fe/BaO–$(TiO_2–BaO)_m$/Co and Fe/$(BaO–TiO_2)_m$/Co structures, respectively.

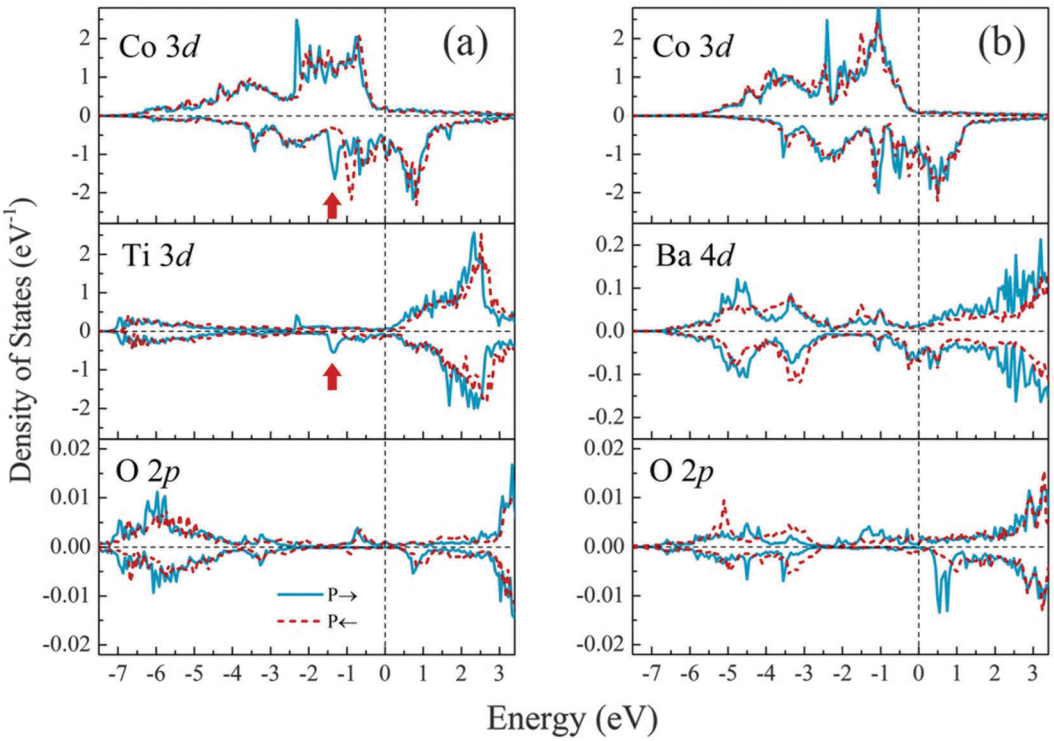

Fig. 8 Orbital-resolved density of states for atoms at (a) Co/TiO_2 interface and (b) Co/BaO interface. The upper and lower panels correspond to majority spin and minority spin, respectively. The vertical dash line indicates the Fermi energy.

intractable to estimate a relatively precise value. Coercive fields show great dependence on the temperature, the film thickness and the electrode. As an amendment, we suggest an interfacial magnetoelectric coefficient α_{MP}, defined as the ratio of the change in the magnetization to the change in electric polarization at the interface, $\alpha_{MP} = \Delta M/\Delta P = (M_+ - M_-)/(P_+ - P_-)$, where M denotes magnetization, P denotes polarization, subscripts + and − denote the parallel and antiparallel orientation with respect to the reference ones. As to each interface, the reference polarization orientation is defined as pointing away from the nearest electrode, while the reference magnetization orientation is defined as the magnetization in the nearest electrode.

Table 1 Difference between the sum of magnetic moments (in units of μ_B) of interfacial atoms for the P→ state and for the P← state

		$\mu_0\Delta M$	
Termination	m	M↑↑	M↑↓
TT	5	87.43	88.78
	6	95.31	94.61
	8	87.01	82.28
	10	127.23	121.35
TB	5	98.22	91.28
	6	91.11	91.64
	7	79.76	70.15
	8	81.54	77.56
BB	6	46.87	43.54
	8	36.04	31.02
	10	31.58	25.32
	12	19.05	15.22
BT	12	31.79	29.31
	13	25.97	24.05
	15	25.55	23.83

Considering the interfacial areas that each contains 1 unit cell of electrodes and 1 unit cell of $BaTiO_3$, the calculated interfacial magnetoelectric coefficients α_{MP} are calculated. Fig. 9 shows the interfacial magnetoelectric coefficients of various interface combinations with film thicknesses greater than CTPB. The all positive values indicate that, at the interface, the magnetization with electric polarization pointing away from the electrode is larger than otherwise. The α_{MP} values at the Fe interface are 50% larger than that at the Co interface, indicating that the influence of the electrode on α_{MP} is more significant and direct than that of others. Given the electrode, α_{MP} at TiO_2 is larger than the BaO interface. Especially at the Co interface, the α_{MP} value of Co/TiO_2 is 300–400% that of the α_{MP} value of the Co/BaO interface. To interpret such interfacial dependence, it is to be noted that the interfacial local polarization is much larger for AO termination than for BO_2 termination, which is the denominator in the formula of α_{MP} calculation. In fact, the magnetization difference contributed by O_{Ba} is nearly equal to Ti. It can be inferred that relatively small α_{MP} of the AO interface results from the large local polarization. As for the influence of the thickness, it is found in Fig. 9 that the α_{MP} value is nearly independent of the ferroelectric film thickness. The abnormal decrease in the α_{MP} value of the Fe/BaO interface results from the non-switchable local polarization, which introduces relatively large error to the calculation of α_{MP}. Since the spin current depends greatly on the

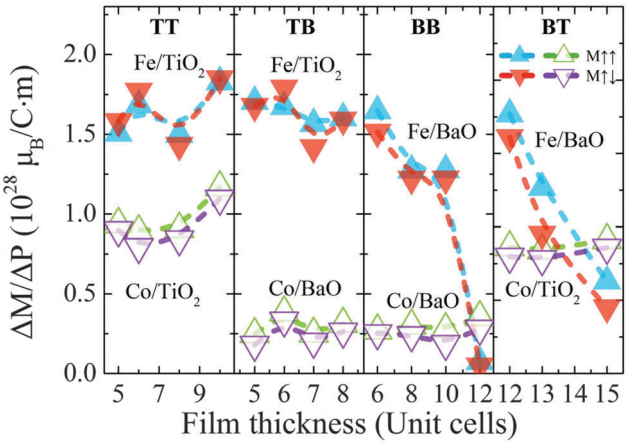

Fig. 9 Interfacial magnetoeletric coefficients for four termination combinations. For each interface, the reference polarization orientation is pointing towards the nearest electrode and the reference magnetization orientation is the magnetization in the nearest electrode.

magnetic state of the system, the magnetoelectric effect suggests a way to acquire a sudden change of spin currents by both electric and magnetic control.

4. Conclusions

In conclusion, we have investigated the interface effect, the size effect and the coupling effect of magnetization and polarization in $Fe/BaTiO_3/Co$ asymmetric multiferroic tunnel junctions using the first-principles simulations based on density functional theory. The equilibrium configurations, polarization, charge density, spin density and magnetic momentums have been comprehensively analyzed in this work. Our results show that ferroelectric stability greatly depends on the combination of the interfaces. The interfacial electric dipole tends to point away from the electrode and the strong short-range interaction may eventually leads to notable collective polarization distortion. The ferroelectric stability is determined as a competition outcome of the strength of short-range chemical bondings and long-range built-in field. In particular, M/BaO termination shows an extraordinary enhancement of local polarization near the interface, especially for the Fe/BaO interface, which exhibits a prominently stable state with an almost "pinned" electric dipole pointing away from the electrode, increasing the critical thickness of ferroelectricity. Apart from the above, the induced magnetic moment on atoms at the interfaces is rather localized and dominated by the local interfacial configuration. In particular, Ti atoms are inclined to be magnetized according to the results that their magnetic moment is induced even in the sub-surface layers, while Ba atoms are opposite. The last but not the least, the induced magnetic moments are significantly altered *via* the reversal of ferroelectric polarization and the difference between the sum of interfacial magnetic moments is enlarged with the increase of the barrier thickness. We suggest that the size effect of asymmetric ferroelectric tunnel junctions should be reconsidered, and traditional phenomenological models should be modified to take into account the details of interfaces to describe the size effect. In general, the modifications of traditional models should appropriately capture the short-range and long-range features of specific interfaces and of their combination. These features (including the interfacial charge transferring, the potential steps, the built-in field, *etc.*) are not only strong functions of the interfacial structure but also coupled with the polarization state of the barrier. Therefore, they cannot be regarded as constants during polarization relaxation.[20] Our results are referential for the manipulation of TMR and TER. We hope our work will stimulate future work on investigation of MFTJs.

Acknowledgements

This work was supported by the National Natural Science Foundation of China (NSFC) (No. 51172291, 11474363, 11232015, 11472313, 11572355). Authors also thank support from the Fundamental Research Funds for the Central Universities, Research Fund for the Doctoral Program of Higher Education (2012017111005, 2013017113003), Fok Ying Tung Foundation, Guangdong Natural Science Funds for Distinguished Young Scholar and China Scholarship Council.

Notes and references

1 M. Bibes, *Nature*, 2008, **7**, 425–426.
2 J. F. Scott, *Nat. Mater.*, 2007, **6**, 256–257.
3 C. Chappert, A. Fert and F. N. Van Dau, *Nat. Mater.*, 2007, **6**, 813–823.
4 V. Garcia, S. Fusil, K. Bouzehouane, S. Enouz-Vedrenne, N. D. Mathur, A. Barthélémy and M. Bibes, *Nature*, 2009, **460**, 81–84.
5 F. Yang, M. H. Tang, Z. Ye, Y. C. Zhou, X. J. Zheng, J. X. Tang, J. J. Zhang and J. He, *J. Appl. Phys.*, 2007, **102**, 044504.
6 J. Mathon and A. Umerski, *Phys. Rev. B: Condens. Mattar Mater. Phys.*, 2001, **63**, 220403.
7 S. Yuasa, T. Nagahama, A. Fukushima, Y. Suzuki and K. Ando, *Nat. Mater.*, 2004, **3**, 868–871.
8 S. Ikeda, J. Hayakawa, Y. Ashizawa, Y. M. Lee, K. Miura, H. Hasegawa, M. Tsunoda, F. Matsukura and H. Ohno, *Appl. Phys. Lett.*, 2008, **93**, 082508.
9 E. Y. Tsymbal and H. Kohlstedt, *Science*, 2006, **313**, 181–183.
10 M. Y. Zhuravlev, R. F. Sabirianov, S. S. Jaswal and E. Y. Tsymbal, *Phys. Rev. Lett.*, 2005, **94**, 246802.
11 X. Luo, Y. Zheng and B. Wang, *J. Appl. Phys.*, 2012, **111**, 074102.
12 J. P. Velev, C. G. Duan, J. D. Burton, A. Smogunov, M. K. Niranjan, E. Tosatti, S. S. Jaswal and E. Y. Tsymbal, *Nano Lett.*, 2009, **9**, 427–432.
13 T. Tybell, C. H. Ahn and J.-M. Triscone, *Appl. Phys. Lett.*, 1999, **75**, 856–858.
14 D. D. Fong, G. B. Stephenson, S. K. Streiffer, J. A. Eastman, O. Auciello, P. H. Fuoss and C. Thompson, *Science*, 2004, **304**, 1650–1653.
15 C. G. Duan, S. S. Jaswal and E. Y. Tsymbal, *Phys. Rev. Lett.*, 2006, **97**, 047201.

16 J. Junquera and P. Ghosez, *Nature*, 2003, **422**, 506–509.
17 Y. Zheng, M. Q. Cai and C. H. Woo, *Acta Mater.*, 2010, **58**, 3050–3058.
18 N. Sai, A. M. Kolpak and A. M. Rappe, *Phys. Rev. B: Condens. Matter Mater. Phys.*, 2005, **72**, 020101.
19 M. Q. Cai, Y. Zheng, P. W. Ma and C. H. Woo, *J. Appl. Phys.*, 2011, **109**, 024103.
20 W. J. Chen, Y. Zheng, X. Luo, B. Wang and C. H. Woo, *J. Appl. Phys.*, 2013, **114**, 064105.
21 X. T. Liu, Y. Zheng, B. Wang and W. J. Chen, *Appl. Phys. Lett.*, 2013, **102**, 152906.
22 J. G. Simmons, *Phys. Rev. Lett.*, 1963, **10**, 10–12.
23 J. G. Simmons, *J. Appl. Phys.*, 1963, **34**, 2581.
24 A. K. Tagantsev, G. Gerra and N. Setter, *Phys. Rev. B: Condens. Matter Mater. Phys.*, 2008, **77**, 174111.
25 G. Gerra, A. K. Tagantsev and N. Setter, *Phys. Rev. Lett.*, 2007, **98**, 207601.
26 Y. Liu, X. P. Peng, X. Lou and H. Zhou, *Appl. Phys. Lett.*, 2012, **100**, 192902.
27 M. Stengel, D. Vanderbilt and N. A. Spaldin, *Nat. Mater.*, 2009, **8**, 392–397.
28 C. G. Duan, J. P. Velev, R. F. Sabirianov, Z. Zhu, J. Chu, S. S. Jaswal and E. Y. Tsymbal, *Phys. Rev. Lett.*, 2008, **101**, 137201.
29 M. Bibes, *Nat. Mater.*, 2012, **11**, 354–357.
30 D. Pantel, S. Goetze, D. Hesse and M. Alexe, *Nat. Mater.*, 2012, **11**, 289–293.
31 D. Cao, H. Shu, Z. Jiao, Y. Zhou, M. Chen, M. Cai and W. Hu, *Phys. Chem. Chem. Phys.*, 2013, **15**, 14770–14776.
32 H. Choi, Y. Hwang, E. K. Lee and Y. C. Chung, *J. Appl. Phys.*, 2011, **109**, 07D909.
33 M. Niranjan, J. Velev, C. G. Duan, S. Jaswal and E. Tsymbal, *Phys. Rev. B: Condens. Matter Mater. Phys.*, 2008, **78**, 104405.
34 J. D. Burton and E. Y. Tsymbal, *Phys. Rev. Lett.*, 2011, **106**, 157203.
35 Y. W. Yin, J. D. Burton, Y.-M. Kim, A. Y. Borisevich, S. J. Pennycook, S. M. Yang, T. W. Noh, A. Gruverman, X. G. Li, E. Y. Tsymbal and Q. Li, *Nat. Mater.*, 2013, **12**, 397.
36 W. Eerenstein, N. D. Mathur and J. F. Scott, *Nature*, 2006, **442**, 759–765.
37 X. Chen, S. Yang, J. H. Kim, H. Do Kim, J. S. Kim, G. Rojas, R. Skomski, H. Lu, A. Bhattacharya, T. Santos, N. Guisinger, M. Bode, A. Gruverman and A. Enders, *New J. Phys.*, 2010, **13**, 083037.
38 G. Kresse and J. Furthmu, *Phys. Rev. B: Condens. Matter Mater. Phys.*, 1996, **54**, 11169–11186.
39 G. Kresse and D. Joubert, *Phys. Rev. B: Condens. Matter Mater. Phys.*, 1999, **59**, 1758–1774.
40 J. P. Perdew and A. Zunger, *Phys. Rev. B: Condens. Matter Mater. Phys.*, 1981, **23**, 5040–5079.
41 X. Luo, B. Wang and Y. Zheng, *ACS Nano*, 2011, **5**, 1649–1656.
42 I. Oleinik, E. Tsymbal and D. Pettifor, *Phys. Rev. B: Condens. Matter Mater. Phys.*, 2001, **65**, 020401.

